Title
Vascular Adaptation of the Right Ventricle in Experimental Pulmonary Hypertension

Journal
American Journal of Respiratory Cell and Molecular Biology, 59(4)

ISSN
1044-1549

Authors
Graham, Brian B
Kumar, Rahul
Mickael, Claudia
et al.

Publication Date
2018-10-01

DOI
10.1165/rcmb.2018-0095oc

Peer reviewed

ORIGINAL RESEARCH

Vascular Adaptation of the Right Ventricle in Experimental Pulmonary Hypertension

Brian B. Graham[1], Rahul Kumar[1], Claudia Mickael[1], Biruk Kassa[1], Dan Koyanagi[1], Linda Sanders[1], Li Zhang[1], Mario Perez[1], Daniel Hernandez-Saavedra[1], Carolyn Valencia[1], Kandice Dixon[2], Julie Harral[2], Zoe Loomis[2], David Irwin[2], Travis Nemkov[3], Angelo D'Alessandro[3], Kurt R. Stenmark[2], and Rubin M. Tuder[1]

[1]Program in Translation Lung Research, Department of Medicine, [2]Department of Pediatrics, and [3]Department of Biochemistry and Molecular Genetics, University of Colorado Denver–Anschutz Medical Campus, Aurora, Colorado

ORCID IDs: 0000-0001-7541-2585 (B.B.G.); 0000-0002-2709-5981 (R.K.); 0000-0001-8566-7119 (T.N.); 0000-0002-2258-6490 (A.D'A.); 0000-0001-6918-6411 (K.R.S.).

Abstract

Optimal right ventricular (RV) function in pulmonary hypertension (PH) requires structural and functional coupling between the RV cardiomyocyte and its adjacent capillary network. Prior investigations have indicated that RV vascular rarefaction occurs in PH, which could contribute to RV failure by reduced delivery of oxygen or other metabolic substrates. However, it has not been determined if rarefaction results from relative underproliferation in the setting of tissue hypertrophy or from actual loss of vessels. It is also unknown if rarefaction results in inadequate substrate delivery to the RV tissue. In the present study, PH was induced in rats by SU5416-hypoxia-normoxia exposure. The vasculature in the RV free wall was assessed using stereology. Steady-state metabolomics of the RV tissue was performed by mass spectrometry. Complementary studies were performed in hypoxia-exposed mice and rats. Rats with severe PH had evidence of RV failure by decreased cardiac output and systemic hypotension. By stereology, there was significant RV hypertrophy and increased total vascular length in the RV free wall in close proportion, with evidence of vessel proliferation but no evidence of endothelial cell apoptosis. There was a modest increase in the radius of tissue served per vessel, with decreased arterial delivery of metabolic substrates. Metabolomics revealed major metabolic alterations and metabolic reprogramming; however, metabolic substrate delivery was functionally preserved, without evidence of either tissue hypoxia or depletion of key metabolic substrates. Hypoxia-treated rats and mice had similar but milder alterations. There is significant homeostatic vascular adaptation in the right ventricle of rodents with PH.

Keywords: pulmonary hypertension; right ventricle; angiogenesis; metabolism

Clinical Relevance

A major determinant of pulmonary hypertension (PH) outcome is right ventricle (RV) function, with some patients adapting well and others progressing to rapid failure despite similar PH severity. Using a measurement approach called stereology, we found rodents with severe PH have significant augmentation of the vascular network in the RV tissue bed, in close proportion to the degree of hypertrophy, which maintains adequate oxygen, glucose, and other metabolic substrate delivery. There was, however, significant RV metabolic reprogramming, consistent with prior reports in PH. These data suggest that there is significant adaptation of the RV vascular network in PH, and the RV metabolic reprogramming may result from intrinsic changes within the cardiomyocytes, rather than substrate deprivation.

(Received in original form March 15, 2018; accepted in final form May 31, 2018)

Supported by National Institutes of Health (NIH) grants R03HL133306, R01HL135872, and P01HL014985 (B.B.G.); the American Thoracic Society Foundation; and the Pulmonary Hypertension Association.

Author Contributions: Conception and design: B.B.G. and R.M.T.; experiments and data acquisition: B.B.G., R.K., C.M., B.K., D.K., L.S., L.Z., M.P., D.H.-S., C.V., K.D., J.H., Z.L., D.I., and T.N.; analysis and interpretation: B.B.G., T.N., A.D'A., and R.M.T.; and drafting of the manuscript for important intellectual content: B.B.G., A.D'A., K.R.S., and R.M.T.

Correspondence and requests for reprints should be addressed to Brian B. Graham, M.D., Program in Translation Lung Research, Department of Medicine, University of Colorado Denver–Anschutz Medical Campus, 12700 East 19th Avenue, C-272, Aurora, CO 80045. E-mail: brian.graham@ucdenver.edu.

This article has a data supplement, which is accessible from this issue's table of contents at www.atsjournals.org.

Am J Respir Cell Mol Biol Vol 59, Iss 4, pp 479–489, Oct 2018

Originally Published in Press as DOI: 10.1165/rcmb.2018-0095OC on May 31, 2018
Internet address: www.atsjournals.org

Right ventricular (RV) failure is the primary cause of death in patients with pulmonary hypertension (PH), but determinants of RV adaptation versus failure are unclear. The manner in which the right ventricle responds in PH is variable, with some individuals progressing toward RV failure and death, whereas others with similar PH severity adapt their RV function more effectively. A prominent example is patients with Eisenmenger's syndrome living decades longer than others with similar PH severity (1–4), likely resulting at least in part from better RV adaptation (5). The mechanisms underlying RV adaptation to PH remain unclear.

Prior studies of RV specimens have identified decreased capillary density in humans with PH and animals with experimental PH (6–18), which has generally been believed to result from vessel loss or dropout. However, reduced vessel density could alternatively result from RV hypertrophy with relatively inadequate angiogenesis. As a consequence of decreased RV vessel density, there could be impaired delivery of oxygen and other metabolic substrates to the RV tissue, which could contribute to cardiac failure (19). In the left ventricle (LV), impaired cardiac angiogenesis precipitates heart failure after aortic banding or induced hypertrophy, but by unclear mechanisms (20, 21). Decreased substrate delivery resulting from RV vascular rarefaction has not been tested experimentally.

We sought to characterize the RV vascular response to PH using design-based stereology, which takes into consideration the absolute tissue volume. This approach allows the quantification of both vascular density relative to the tissue volume and assessment of absolute vascular length in the tissue bed. We primarily used the SU5416-hypoxia-normoxia rat model, which results in progressive PH and RV failure. We found rodents with this experimental PH had a significant increase in absolute RV vascular length, which was in close correlation with but slightly less than the degree of hypertrophy, resulting in relative vascular rarefaction. When coupled with observations of significant RV angiogenesis and no evidence of vessel apoptosis, we interpret RV rarefaction as resulting from underproliferation in the setting of hypertrophy. By complementary metabolomic analysis of the RV tissue, we found extensive metabolic reprogramming in the RV tissue but no evidence of inadequate oxygen or other metabolic substrate delivery.

Methods

Animal Models

All animal experiments were approved by the University of Colorado Institutional Animal Care and Use Committee. Female Sprague-Daley rats (Taconic Biosciences) 6–8 weeks of age received subcutaneous 20 mg/kg SU5416 (Tocris Bioscience) dissolved in carboxymethylcellulose (CMC) and then diluted in 1:1 with PBS, or the equivalent volume of vehicle alone, and then hypobaric normoxia (equivalent altitude of 5,500 m, or 10% $F_{I_{O_2}}$) for 21 days' duration or adjacent ambient chambers, followed by ambient air for an additional 2 or 5 weeks. At the conclusion of the experiment, the rats underwent terminal RV catheterization under anesthesia with inhaled isoflurane with placement of a Millar catheter into the jugular vein and advanced into the right ventricle, followed by RV tissue collection. Some of the animals were given intraperitoneal injection with 60 mg/kg pimonidazole hydrochloride (Hypoxyprobe; NPI) 1 hour before being killed. At the time of heart catheterization, some of the animals received 300 μl of 10-μm fluorescent beads (Invitrogen) injected into the LV for quantification of regional tissue perfusion. We also exposed female C57BL6/J mice (The Jackson Laboratory) at 6 weeks of age to 10% $F_{I_{O_2}}$ for 7 days' duration or *Schistosoma mansoni* eggs, compared with untreated control mice. Further details are provided in the Supplemental Methods section of the data supplement.

Tissue Analysis

The tissue-processing approach is shown in Figure E1 in the data supplement. Rat RV free wall tissue volume was determined by water displacement. Mouse RV free wall tissue volume was determined by dividing RV mass by cardiac tissue density (1.06 g/cm^3 as previously reported [22], and similar to that calculated for a human specimen) (Figure E2). The RV tissue stereology approach is described in the Supplemental Methods section of the data supplement and shown in Figure E1C. Formalin-fixed, paraffin-embedded sections were stained using the reagents and protocols in Table E1, and snap-frozen tissue was homogenized and probed by Western blotting using the reagents and protocols reported in Table E2. Metabolite analysis was performed on snap-frozen samples of rat and mouse RV tissue by mass spectrometry, as previously reported (23); further details are described in the Supplemental Methods section of the data supplement. Arterial blood metabolites were quantified using the approaches reported in Table E3.

Results

We challenged rats with the vascular endothelial growth factor (VEGF) receptor 2 inhibitor SU5416 in combination with 3 weeks of hypoxia, followed by an additional 5 weeks of normoxia (abbreviated SU-Hx+5; diagrammed in Figure 1A), as previously reported (24). It has been described that the PH phenotype continues to progress for up to 10 weeks of normoxia (25); however, at Denver elevation (1,600 m; equivalent to 19% $F_{I_{O_2}}$ at sea level), we observed mortality in this model starting at 5 weeks after reexposure to normoxia. PH animals were compared with vehicle (CMC)-treated animals maintained in normoxia for the same duration of time (abbreviated CMC-Nx+5). RV catheterization revealed a significantly higher pressure in the diseased animals (Figure E3A), although 3 of the 14 animals died of hemodynamic instability during RV catheterization. Furthermore, we observed that cardiac output and systemic blood pressure were decreased, RV systolic and diastolic chamber volumes were increased, and there was an increase in arterial blood lactate in the diseased rats (Figures E3B–E3F). These results were consistent with significant cardiac failure in end-stage PH.

The RV free wall was resected, and the absolute volume of the tissue was determined by water displacement (Archimedes' principle) (Figure E1A). We observed that there was a significant increase in the RV free wall volume in the diseased rats compared with control rats (Figure 1B), consistent with RV hypertrophy. We then measured the absolute length of the vasculature in the RV free wall (largely represented by capillaries) by stereology (26) (Figures E1B and E1C). We observed a significant increase in the absolute vascular length in the diseased animals compared with the control animals (Figure 1C). There

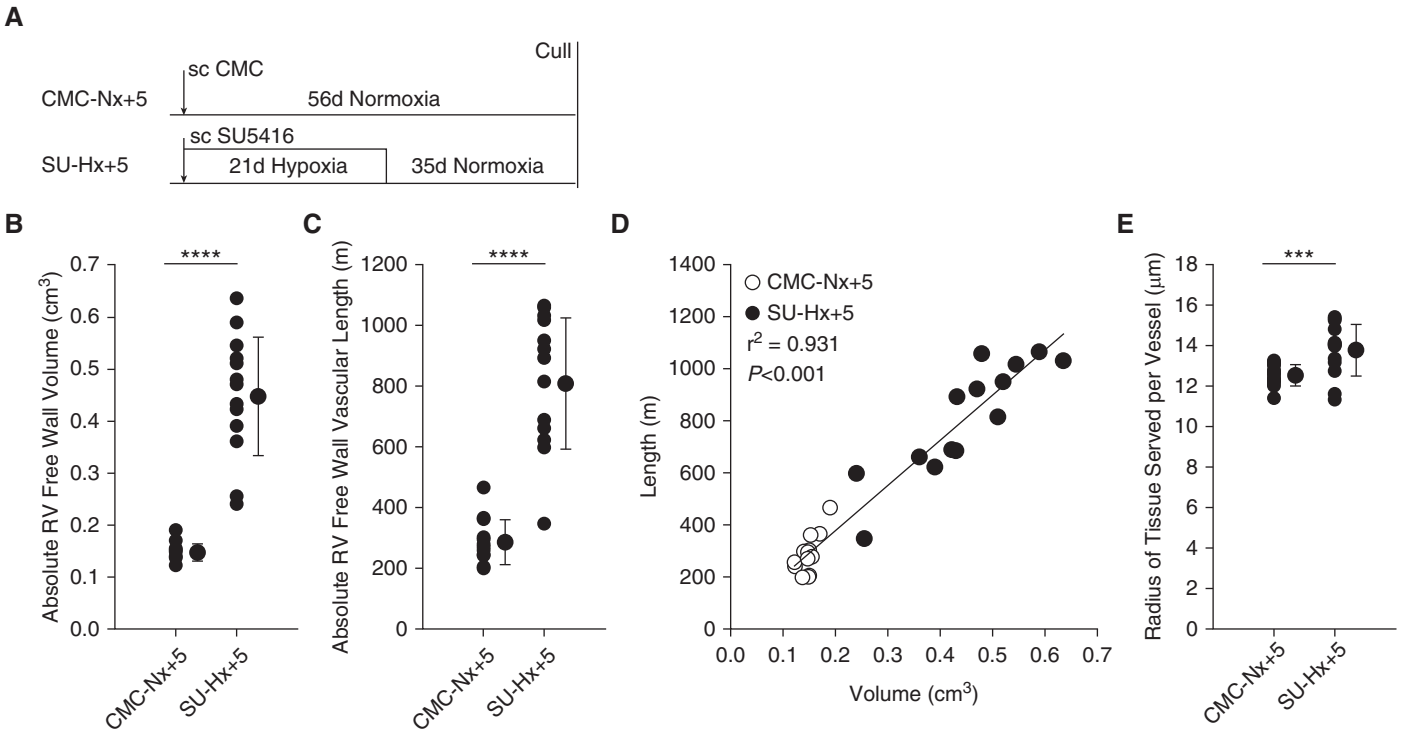

Figure 1. Rats with severe SU5416-hypoxia (SU-Hx)-induced pulmonary hypertension (PH) have a significant increase in total right ventricular (RV) vascular length, which correlates with an increase in RV volume. (*A*) Schematic of models. (*B*) RV free wall absolute volume ($n = 14$–15/group; rank-sum test). (*C*) RV free wall absolute vascular length ($n = 14$/group; rank-sum test). (*D*) Correlation of RV volume and vascular length (linear regression; $n = 14$/group). (*E*) Radius of RV tissue served per vessel ($n = 14$/group; rank-sum test). *B*, *C*, and *E* show mean ± SD plotted values. ***$P < 0.005$; ****$P < 0.001$. CMC = carboxymethylcellulose; CMC-Nx+2 = carboxymethylcellulose and 5 total weeks of normoxia; CMC-Nx+5 = carboxymethylcellulose and 8 total weeks of normoxia; Nx = normoxia; sc CMC = subcutaneous carboxymethylcellulose; sc SU5416 = subcutaneous SU5416; SU-Hx+2 = SU5416 with 3 weeks of hypoxia and 2 weeks of normoxia; SU-Hx+5 = SU5416 with 3 weeks of hypoxia and 5 weeks of normoxia.

was a tight correlation between absolute RV volume and absolute RV vascular length ($R^2 = 0.931$; $P < 0.001$) (Figure 1D), consistent with adaptation of the vasculature in the setting of RV hypertrophy.

We calculated the average radius of cross-sectional RV tissue served per vessel as a quantitative measure of the minimum distance for oxygen and other metabolites to diffuse from cardiac capillaries to cardiomyocytes. We observed that this effective diffusion radius was modestly but significantly greater in the diseased animals, increasing from 12.6 μm (median; 12.2–13.1 interquartile range) in the control animals to 14.1 μm (13.1–14.9) in the PH animals, an increase of 1.5 μm ($P = 0.004$ by rank-sum test) (Figure 1E).

To broaden the scope of our studies, we compared three additional groups of rats with experimental PH versus appropriate controls: *1*) SU5416-hypoxia-normoxia at an earlier, more compensated time point (at 2 weeks after reexposure to normoxia, designated SU-Hx+2); *2*) vehicle treatment followed by hypoxia for 3 weeks and then 2 weeks of normoxia (designated CMC-Hx+2); *3*) SU5416 treatment followed by normoxia for the same total of 5 weeks (designated SU-Nx+2); and *4*) vehicle treatment alone for the same total period of time (designated CMC-Nx+2). We observed that both the SU-Hx+2 and CMC-Hx+2 experimental groups had significant increases in RV volume and RV vascular length (Figure E4), but only the SU-Hx+2 group had a significant increase in the radius of tissue served per vessel. Interestingly, the radius in the normotensive control animals (i.e., with normal RV function and structure) also increased because the animals were 3 weeks older (comparing the CMC-Nx+2 with the CMC-Nx+5 groups), to a degree similar to that induced by SU-Hx exposure at either time point. The SU-Nx+2 animals did not have a significant phenotype, with a mild but nonsignificant increase in RV pressures and no evidence of RV hypertrophy or RV vascular augmentation.

Having identified an increase in total RV vascular length in the SU5416-hypoxia-normoxia (SU-Hx-Nx) rats, consistent with angiogenesis, we sought evidence of vascular proliferation. We observed that at the earlier time point (in the SU-Hx+2 group), there was a significant increase in endothelial cell nuclear profiles that costained for proliferating cell nuclear antigen; endothelial cell proliferation subsequently decreased in animals at the later time point (the SU-Hx+5 group) (Figures 2A and 2B). We also sought to identify if there was evidence of apoptosis in the RV tissue, which could result in vascular "dropout" or rarefaction, using TUNEL staining, but we found no evidence of apoptosis in the RV tissue at either the early or the late time points (Figures 2C and 2D). We quantified the expression of VEGF, which is the prototypical driver of angiogenesis, particularly when triggered by regional hypoxia. However, we observed no change in VEGF expression in the RV tissue of the diseased rats (Figure E5).

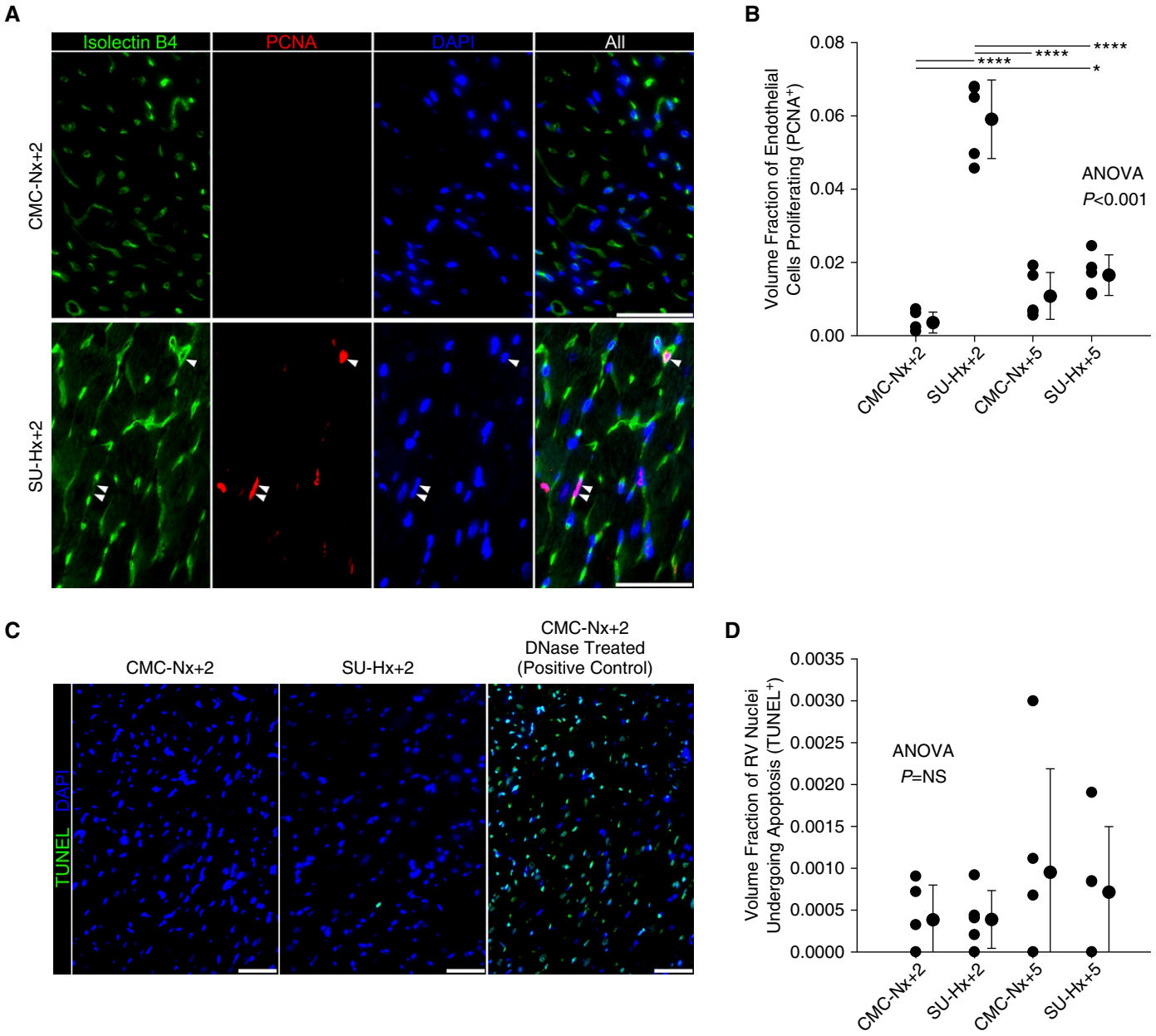

Figure 2. RV endothelial cells are proliferating in SU-Hx rats, and there is no evidence of apoptosis. (*A*) Representative images of CMC-Nx+2 and SU-Hx+2 rat RV tissue immunostained for lectin and proliferating cell nuclear antigen (PCNA; $n = 5$/group; white arrowheads mark PCNA$^+$ endothelial cells; scale bars = 50 μm). (*B*) Quantification of the volume fraction of endothelial cell nuclei that are also PCNA positive ($n = 5$/group; mean ± SD plotted; ANOVA with *post hoc* Tukey test). (*C*) Representative images of CMC-Nx+2 and SU-Hx+2 rat RV tissue stained by TUNEL assay, with a DNase-treated specimen shown as a positive control ($n = 5$/group; scale bars = 50 μm). (*D*) Quantification of volume fraction of all RV nuclei that are also TUNEL positive ($n = 5$/group; mean ± SD plotted; ANOVA P = NS). *$P < 0.05$; ****$P < 0.001$. NS = not significant.

Perfusion of the RV free wall was determined by multiplying total cardiac output by the fraction of cardiac output delivered to the right ventricle, measured by quantifying the fraction of microspheres injected into the left ventricular cavity that deposited into the RV tissue bed. As noted above, total cardiac output was decreased in the rats with severe, end-stage PH (Figure E3B). We observed that total perfusion of the RV free wall was similar between the control and diseased animals (Figure 3A), but after correcting for RV hypertrophy, calculated perfusion per cubic micrometer of RV tissue was significantly less in the diseased animals (Figure 3B). These results are consistent with the multiplicative product of decreased cardiac output and vascular rarefaction.

We then calculated the arterial delivery of glucose and free fatty acids to the RV tissue bed by measuring the concentration of these metabolites in arterial blood (Figures E6A and E6B) and multiplying the concentrations by RV tissue perfusion. We observed that delivery of free fatty acids per unit volume of RV tissue was significantly decreased, and there was a strong trend

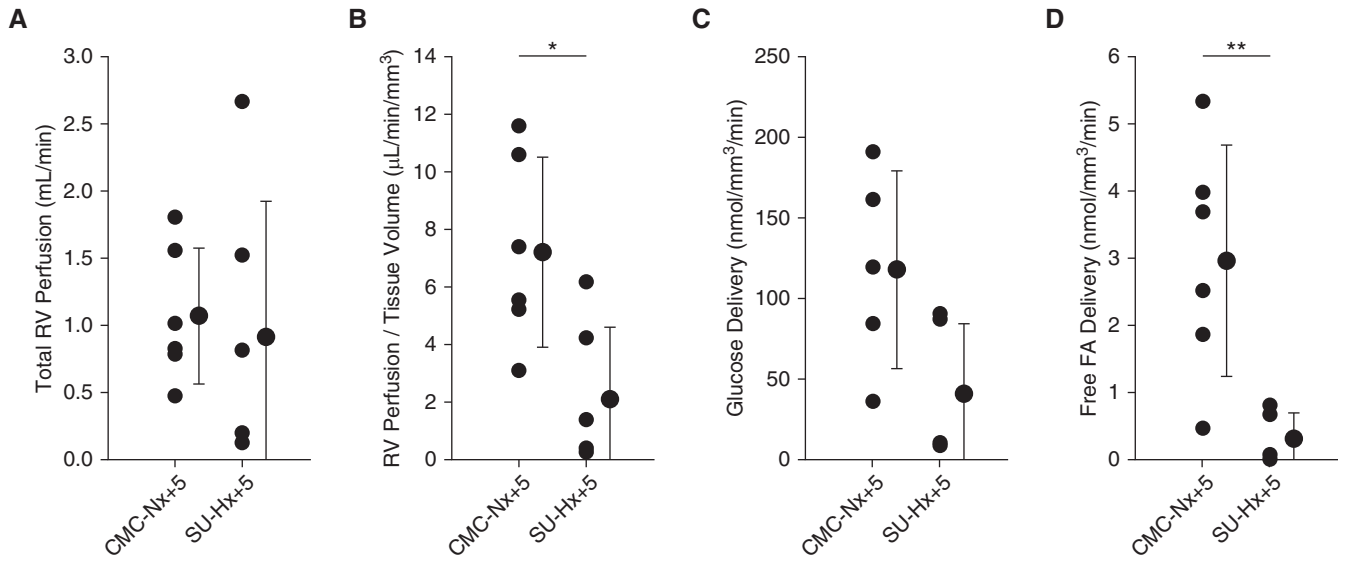

Figure 3. Rats with severe SU-Hx-induced pulmonary hypertension have less RV tissue perfusion and metabolite delivery when corrected for hypertrophy. (*A*) Total RV free wall perfusion and (*B*) RV perfusion per unit volume of tissue, calculated by multiplying absolute cardiac output by the fraction of microbeads administered via the left ventricle that deposited in the right ventricle free wall ($n = 6$/group; *t* test). (*C* and *D*) Arterial blood delivery of (*C*) glucose and (*D*) free fatty acids to the right ventricle free wall tissue bed, calculated by multiplying arterial blood metabolite content by perfusion ($n = 5$–6/group; *t* test; mean ± SD plotted). $^*P < 0.05$; $^{**}P < 0.01$. FA = fatty acids.

($P = 0.0508$) toward decreased glucose delivery as well in animals with severe PH as compared with the control animals (Figures 3C and 3D). We also assessed the concentrations and delivery of glutamine and glutamate (alternative metabolic substrates, which may have increased uptake into the PH right ventricle [27]), and we found that the delivery of these two amino acids to the RV free wall was also decreased (Figures E6C–E6F). These findings are consistent with the assessments of RV blood flow outlined above.

We sought to determine if there was evidence of functionally inadequate delivery of oxygen to the RV tissue by assaying for tissue-level hypoxia after pimonidazole hydrochloride (Hypoxyprobe; NPI) administration. Pimonidazole is highly diffusible and forms adducts in settings of local P_{O_2} less than or equal to 10 mm Hg (28). Using as a positive control the hypoxia present in the center of murine peri-*Schistosoma* egg granulomas (Figure E7), which we had previously observed by immunohistochemistry (29), we did not find significant pimonidazole binding in RV tissue from either control or PH rats by immunostaining (Figure 4). In the few RV specimens that had positive signal, the intensity was relatively homogeneous. We also did not find differences in pimonidazole binding by Western blotting at the later time point (Figure E8).

We then sought to determine if there was evidence of functionally inadequate delivery of other metabolic substrates to the RV tissue by steady-state metabolomic analysis using mass spectrometry on SU-Hx+5 and CMC-Nx+5 right ventricle specimens. Overall, we observed major differences in the RV content of many metabolites between the diseased and control tissues, with separation into two distinct groups by principal component analysis (Figures 5A and 5B). Metabolomic network pathway analysis was performed to identify pathways that were altered in the diseased RV tissue (graphical representation in Figure E9, with the list of pathways given in Table E4). Notably, the major metabolic changes included pathways and specific increases in markers of protein/amino acid catabolism (including citrulline, proline, hydroxyproline, and guanidinoacetate) in the PH group compared with the control group (Figure E10A). There was also an increase in the ratio of glutathione relative to glutathione disulfide, indicative of increased use of the pentose phosphate pathway, and a decrease in γ-glutamyl peptide concentration indicative of increased γ-glutamyl cycle activity—both findings indicative of upregulated protective mechanisms against oxidant damage (Figure E10B). The trichloroacetic acid (TCA) cycle was also altered in the diseased tissue, and specifically we found decreases in the carboxylic acids α-ketoglutaric acid and malate, indicating citric acid cycle intermediate depletion, and the total adenylate pool (ATP, ADP, AMP) was also decreased, all consistent with a deregulation of mitochondrial metabolism (Figure E11; the full rat RV metabolomics dataset is provided in Table E5).

Despite these significant metabolic changes, we did not find evidence of substrate depletion when we focused on metabolic substrates in particular—the most proximate metabolites that feed downstream metabolic pathways. There was no change between the two groups in the concentration of glucose or pyruvate, and there was no significant increase in lactate production, which would be predicted to occur if the RV cardiomyocytes were hypoxic (Figures 5C–5E). There was also no evidence of hydroxybutyrate depletion, a ketone body deriving from lipid oxidation (Figure 5F). Finally, we also did not observe significant decreases in the RV content of glutamine or glutamate, amino acids that can replenish the citric acid cycle (anaplerosis) (Figure 5G). None of these substrate concentrations had a trend toward a difference between the two groups, because all *t* test *P* values comparing the PH and control groups were greater than 0.20.

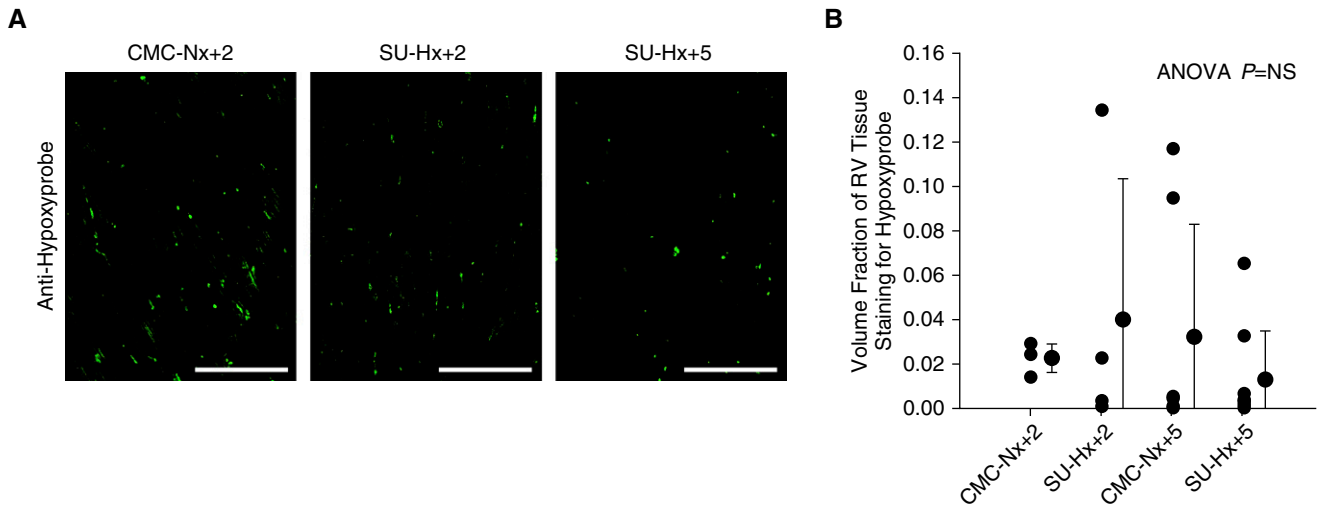

Figure 4. No evidence of RV tissue hypoxia by hypoxyprobe binding. (*A*) Representative antihypoxyprobe immunostaining in animals that received intraperitoneal hypoxyprobe before being killed (scale bars = 100 μm). (*B*) Quantification by volume density using stereology (n = 4–9/group; mean ± SD plotted).

We sought to confirm our findings using another rodent model of PH, hypoxia-exposed mice. We used the 7-day time point, as previously described by Kolb and colleagues (30). We reproduced these results, observing increases in both RV volume and total RV vascular length, which significantly and closely correlated with each other (Figures 6A–6C). There was no significant change in the radius of tissue served per vessel with this milder model of PH (Figure 6D). There was an increase in proliferating cell nuclear antigen–positive endothelial cells (Figure 6E), confirming the report of increased Ki-67–positive endothelial cells by flow cytometry (30), without evidence of apoptosis in murine RV tissue (Figure 6F). As in the rat model, steady-state RV content of key metabolic substrates, including glucose, pyruvate, lactate, glutamine, and glutamate, was not altered in the mice with hypoxia-induced PH compared with control mice (Figures 6G–6J); hydroxybutyrate was not detected. There was also substantially less derangement of downstream substrate use (Figure E12).

We also analyzed a second mouse model of PH, triggered by *S. mansoni*, which we had previously developed (29, 31). In this model of PH, however, we did not find a significant change in RV volume, and there was no evidence of vascular adaptation (Figures E13A–E13E). *Schistosoma*-exposed mice also had no evidence of substrate depletion, although there was an increase in RV lactate content (Figures E13F–E13I). Interestingly, there was an increase in ATP and other metabolites in the RV tissue, consistent with a well-functioning right ventricle (Figure E14; the full RV metabolomics dataset for hypoxia and *Schistosoma*-PH mice is provided in Table E6).

Discussion

We performed rigorous stereologic analysis of the vasculature in the RV free wall tissue of rats with severe experimental PH induced by SU-Hx-Nx exposure. We observed significant and tightly correlated increases in both the volume of the tissue bed and the absolute length of the vascular network (3.0-fold and 2.8-fold increases, respectively, in the SU-Hx+5 animals compared with the CMC-Nx+5 controls). The increased vascular length was the result of significant endothelial cell proliferation, consistent with angiogenesis.

Rarefaction of the right ventricle vascular network has been described in human PH specimens and models of PH (6–18). We found that the slightly smaller fold change in vascular length as compared with the degree of RV hypertrophy resulted in a modest but statistically significant decrease in vascular density, with a 1.5-μm increase in the radius of tissue served per vessel. This rarefaction likely resulted from underproliferation rather than vessel loss or dropout, because no apoptosis was observed. This degree of rarefaction is similar to that observed in end-stage human tissue specimens, which we recently reported to be 2.5 μm using similar techniques (18). Of note, the 2.8-fold increase in absolute vascular length in the rats with experimental PH observed in the present study was greater than the 1.9-fold greater absolute vascular length in the diseased human specimens than in the control human specimens, suggesting that rat right ventricles with this shorter disease course may have a greater capacity for adaptation than human right ventricles in chronic PH. The key RV stereologic parameters obtained from previously analyzed human specimens (18) and the rat and mouse experimental PH models used in the present study are summarized in Table E7.

The diffusion distance of oxygen in tissue is less than or equal to 170 μm (32), making it unlikely that the 1.5- to 2.5-μm degree of rarefaction results in ischemia. Indeed, we did not detect evidence of tissue-level hypoxia, observing no change in pimonidazole (Hypoxyprobe; NPI) binding. Pimonidazole has potential limitations as a probe for tissue hypoxia. It can undergo oxidative metabolism, resulting in nonbinding derivatives that are excreted, which could result in a falsely decreased signal (28). Furthermore, the local P_{O_2}, which regulates pimonidazole adduct formation, reflects both O_2 delivery by the circulation and O_2 consumption, such as by mitochondrial respiration: Parallel changes in both delivery and consumption could result in an incorrect interpretation of the pimonidazole binding signal. However, the

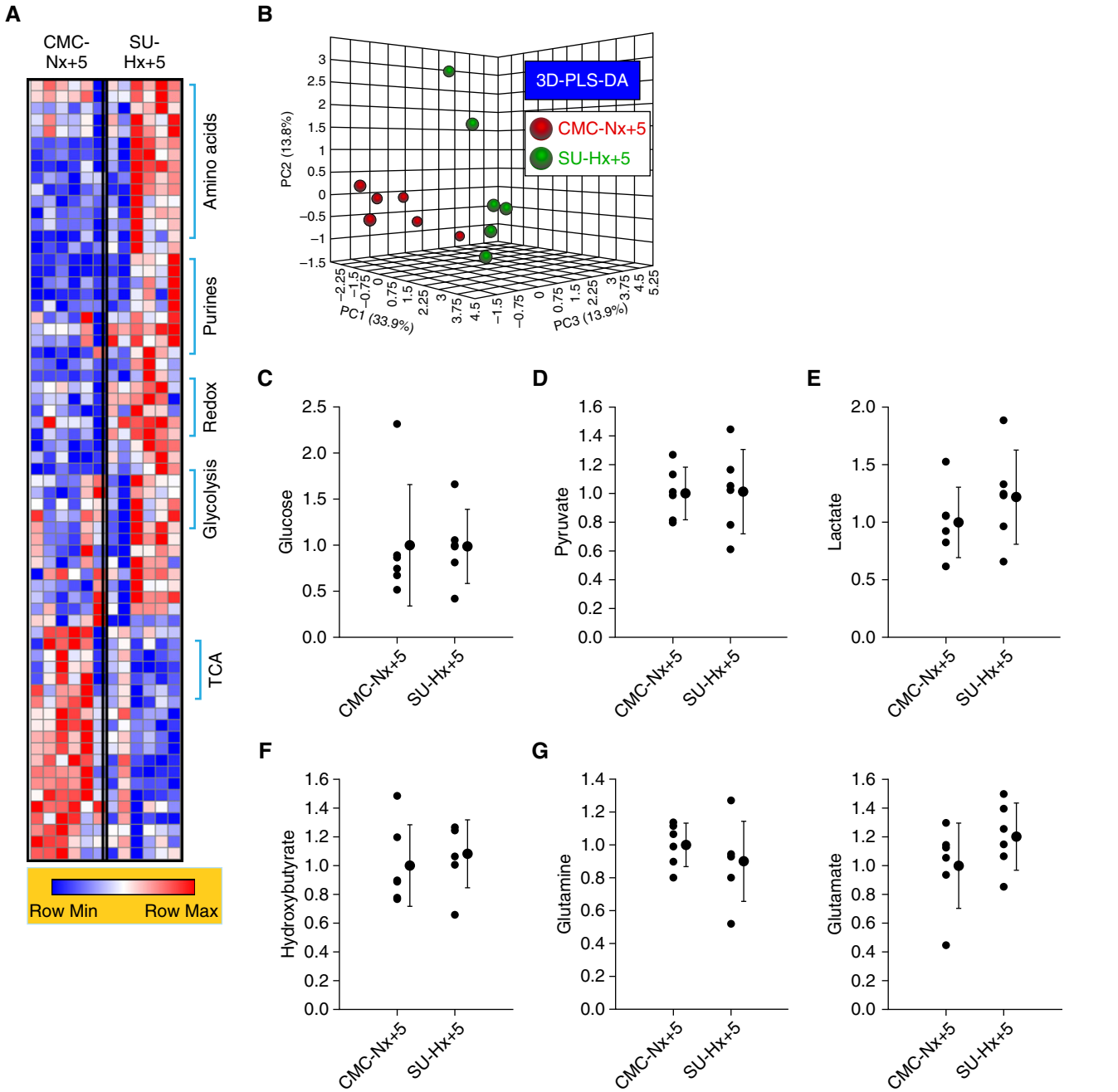

Figure 5. Despite major changes in the overall RV metabolic state assessed by metabolomics, key metabolic substrates are not depleted in the RVs of SU-Hx+5 rats compared with CMC-Nx+5 rats. (*A*) Graphical depiction of right ventricular metabolite content in the two groups ($n = 6$/group). (*B*) Principal component (PC) analysis of the CMC-Nx+5 and SU-Hx+5 groups. (*C*) Glucose. (*D*) Pyruvate. (*E*) Lactate. (*F*) Hydroxybutyrate, a ketone body. (*G*) The amino acids glutamine and glutamate, alternative sources of carbon for anaplerosis. ($N = 6$/group; results in *C–G* are normalized to mean of CMC-Nx+5 group = 1; mean ± SD plotted; *t* test P = NS for all metabolic substrate comparisons in *C–G*.) 3D-PLS-DA = 3-dimensional partial least squares discriminant analysis; PC1, 2, and 3 = principal components 1, 2, and 3; TCA = trichloroacetic acid.

absence of hypoxyprobe binding was corroborated by no increase in VEGF expression and no increase in lactate content in the diseased RV tissue, both of which would be expected if there was regional hypoxia. Interestingly, the degree of RV vascular rarefaction was comparable to that resulting from 3 weeks of additional age in normotensive rats and could be related to increases in pulmonary pressure with age such as that seen in normal humans (33).

Although VEGF is the prototypical driver of angiogenesis, the RV vascular adaptation observed in the present study is likely driven by a VEGF-independent mechanism, because we observed no change in VEGF expression, similar to prior reports

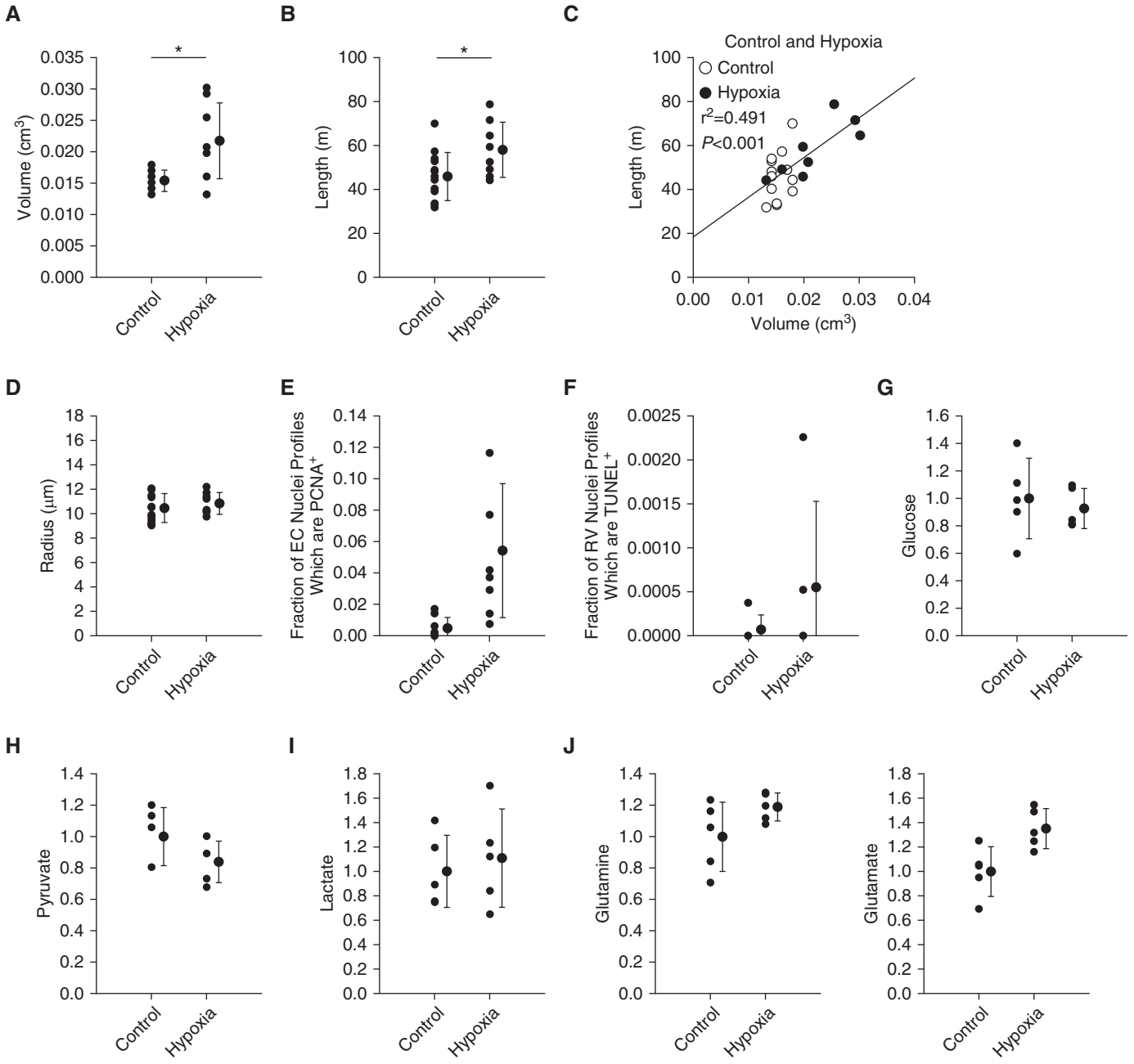

Figure 6. Mice with hypoxia-induced PH also have RV vascular adaptation, without evidence of depletion of key RV metabolic substrates. (*A*) RV volume ($n = 8$–13/group; mean ± SD plotted; rank-sum test). (*B*) Total RV vascular length ($n = 8$–13/group; mean ± SD plotted; *t* test). (*C*) Correlation of RV volumes and total vascular length (linear regression; $n = 8$–13/group). (*D*) Radius of tissue served per vessel ($n = 8$–13/group; mean ± SD plotted; *t* test P = NS). (*E*) Quantification of fraction of endothelial cell (EC) nuclei that are also PCNA positive ($n = 8$/group; mean ± SD plotted; rank-sum test P = NS). (*F*) Quantification of fraction of all RV cell nuclei that are also TUNEL positive ($n = 5$/group; mean ± SD plotted; rank-sum test P = NS). Content of metabolites in RV tissue: (*G*) glucose; (*H*) pyruvate; (*I*) lactate; (*J*) the amino acids glutamine and glutamate ($n = 5$/group; results normalized to mean of control group = 1; mean ± SD plotted; *t* test P = NS for all except as shown). $^*P < 0.05$. Control = Normoxia; Hypoxia = 7 days hypoxia.

in monocrotaline-treated rats and hypoxia-treated mice (13, 30). There are undoubtedly paracrine cytokines or chemokines or direct cell–cell communication that links cardiomyocytes with endothelial cells to maintain vascular density homeostasis by molecular feedback loops yet to be defined. We cannot exclude a potential role for VEGF earlier in the adaptation course, and VEGF could well be important in RV vascular adaptation of other models of PH. Alternative candidate signaling molecules that could maintain the tight structural coupling between cardiomyocytes and capillaries include

fibroblast and hepatocyte growth factors, ephrins, angiopoietins, and metabolites (19). Capillary growth requires endothelial cell glycolysis mediated by HIF-1α (hypoxia-inducible factor-1α) stabilization and expression of PFKFB3 (phosphofructokinase-2/fructose-2,6-bisphosphatase 3) (34, 35); deletion of endothelial cell HIF-1α expression blocks left ventricular vascular adaptation after aortic banding (20), and it may also be critical for RV vascular adaptation. After infarction, cardiac angiogenesis results from clonal proliferation of endothelial cells (36), although it is unclear if the same mechanisms underlie angiogenesis in the absence of frank ischemia.

We did observe major changes in the concentrations of many metabolites in the RV tissue from the three PH models we analyzed (SU-Hx+5 rats, hypoxia-PH mice, and *Schistosoma*-PH mice). Both the rat and hypoxic mouse models had dysregulation of TCA cycle intermediates, which was more profound with the more severe PH in the rat model; there were also decreases in ATP, ADP, and AMP in the rats. These data are consistent with a shift to increased glycolysis rather than oxidative phosphorylation, as has previously been suggested by increased uptake of ^{18}F-fluorodeoxyglucose (37–40), which results in less ATP production per mole of substrate. The *Schistosoma*-PH model, with a milder PH phenotype, however, had an increase in several TCA cycle intermediates, as well as an increase in RV ATP content, suggestive of maintained or even upregulated oxidative phosphorylation. Our data suggest that this extensive metabolic reprogramming is likely driven by intrinsic alterations at the level of the cardiomyocytes, such as triggered by increased afterload and work, rather than a consequence of a functional imbalance between energetic demands and delivery of oxygen or other metabolic substrates. Although we did find reduced glucose, fatty acid, glutamine, and glutamate delivery to the RV tissue, resulting from decreased cardiac output with RV failure compounded by the reduction in vascular density observed, in none of the models did we find evidence of substrate depletion within the tissue bed itself.

A current framework for considering RV performance in PH is early adaptation followed by late maladaptation (8, 19). However, there are many structural and functional characteristics that change along the spectrum of adaptation to maladaptation, and at any given point, some aspects may be more compensated and other aspects more decompensated, rather than manifesting as a binary transition. In early and mild PH, RV homeostasis is maintained, including cardiomyocyte hypertrophy and adaptation of the vascular network to maintain its function of metabolic delivery. As the disease continues, homeostatic programs will not be able to continue adapting indefinitely, restricting further adaptation; furthermore, new pathobiologic programs will be activated that drive RV failure. In the present study, in rats with severe PH and failing right ventricles, we found evidence of significant RV vascular augmentation with a mildly reduced density. We suggest that this near maintenance of homeostasis should be interpreted as more adapted than maladapted along the spectrum. This interpretation is supported by the findings of increased RV capillary to myocyte radius in older versus younger normal rats.

We also found decreased metabolic substrate delivery to the RV tissue bed, which could be interpreted as the result of the product of decreased cardiac output and decreased vascular density. However, we found no evidence that change in vascular structure adversely affects RV function in these animal models of PH, because there was no evidence of substrate depletion or tissue hypoxia. An interpretation of these data is that the healthy RV tissue bed has a functional reserve, resulting from basal overcapacity in vascular density and metabolite delivery; in disease, the observed reduction in vascular density and substrate delivery appears to be within the functional reserve capacity of the tissue.

Rather than vascular rarefaction and decreased substrate delivery, a major driver of RV maladaptation may be modifications within the cardiomyocytes. Changes in cardiomyocyte fatty acid metabolism result in decreased fatty acid transport to the mitochondria and reduced β-oxidation, as well as in increased ceramides and lipid droplet formation (41, 42); modifying fatty acid metabolism directly with a peroxisome proliferator-activated receptor-γ agonist may improve the RV phenotype (43). Furthermore, intrinsic changes in the RV cardiomyocyte contractile apparatus have been described in patients with scleroderma-associated pulmonary arterial hypertension (44). The rapid recovery in RV function starting immediately after allograft placement in lung transplant for PH (45) is too fast for changes in RV structure, and it may be more consistent with reversal of intrinsic cardiomyocyte pathologies.

In summary, we observed that rats with severe experimental PH have significant augmentation of their RV vasculature in the setting of RV hypertrophy. We did not find evidence of functionally inadequate delivery of oxygen or other metabolic substrates to the RV tissue. These findings are consistent with significant homeostatic vascular adaptation. ■

Author disclosures are available with the text of this article at www.atsjournals.org.

Acknowledgment: Schistosome-infected mice were provided by the National Institute of Allergy and Infectious Diseases (NIAID) Schistosomiasis Resource Center at the Biomedical Research Institute (Rockville, MD) through NIH-NIAID contract HHSN272201000005I for distribution through BEI Resources.

References

1. Hjortshøj CMS, Kempny A, Jensen AS, Sørensen K, Nagy E, Dellborg M, *et al*. Past and current cause-specific mortality in Eisenmenger syndrome. *Eur Heart J* 2017;38:2060–2067.
2. Clavé MM, Maeda NY, Castro CRP, Bydlowski SP, Lopes AA. Factors influencing outcomes in patients with Eisenmenger syndrome: a nine-year follow-up study. *Pulm Circ* 2017;7: 635–642.
3. Hascoet S, Fournier E, Jaïs X, Le Gloan L, Dauphin C, Houeijeh A, *et al*. Outcome of adults with Eisenmenger syndrome treated with drugs specific to pulmonary arterial hypertension: a French multicentre study. *Arch Cardiovasc Dis* 2017;110:303–316.
4. Körten MA, Helm PC, Abdul-Khaliq H, Baumgartner H, Kececioglu D, Schlensak C, *et al*.; Competence Network for Congenital Heart Defects Investigators. Eisenmenger syndrome and long-term survival in patients with Down syndrome and congenital heart disease. *Heart* 2016;102:1552–1557.

5. Moceri P, Bouvier P, Baudouy D, Dimopoulos K, Cerboni P, Wort SJ, *et al*. Cardiac remodelling amongst adults with various aetiologies of pulmonary arterial hypertension including Eisenmenger syndrome—implications on survival and the role of right ventricular transverse strain. *Eur Heart J Cardiovasc Imaging* 2017;18: 1262–1270.
6. Al-Husseini A, Kraskauskas D, Mezzaroma E, Nordio A, Farkas D, Drake JI, *et al*. Vascular endothelial growth factor receptor 3 signaling contributes to angioobliterative pulmonary hypertension. *Pulm Circ* 2015;5:101–116.
7. Bogaard HJ, Natarajan R, Henderson SC, Long CS, Kraskauskas D, Smithson L, *et al*. Chronic pulmonary artery pressure elevation is insufficient to explain right heart failure. *Circulation* 2009;120: 1951–1960.
8. Ryan JJ, Huston J, Kutty S, Hatton ND, Bowman L, Tian L, *et al*. Right ventricular adaptation and failure in pulmonary arterial hypertension. *Can J Cardiol* 2015;31:391–406.
9. Poels EM, Bitsch N, Slenter JM, Kooi ME, de Theije CC, de Windt LJ, *et al*. Supplementing exposure to hypoxia with a copper depleted diet does not exacerbate right ventricular remodeling in mice. *PLoS One* 2014;9:e92983.
10. Drake JI, Bogaard HJ, Mizuno S, Clifton B, Xie B, Gao Y, *et al*. Molecular signature of a right heart failure program in chronic severe pulmonary hypertension. *Am J Respir Cell Mol Biol* 2011;45:1239–1247.
11. Alzoubi A, Toba M, Abe K, O'Neill KD, Rocic P, Fagan KA, *et al*. Dehydroepiandrosterone restores right ventricular structure and function in rats with severe pulmonary arterial hypertension. *Am J Physiol Heart Circ Physiol* 2013;304:H1708–H1718.
12. Bogaard HJ, Mizuno S, Hussaini AAA, Toldo S, Abbate A, Kraskauskas D, *et al*. Suppression of histone deacetylases worsens right ventricular dysfunction after pulmonary artery banding in rats. *Am J Respir Crit Care Med* 2011;183:1402–1410.
13. Potus F, Ruffenach G, Dahou A, Thebault C, Breuils-Bonnet S, Tremblay È, *et al*. Downregulation of microRNA-126 contributes to the failing right ventricle in pulmonary arterial hypertension. *Circulation* 2015;132:932–943.
14. Sutendra G, Dromparis P, Paulin R, Zervopoulos S, Haromy A, Nagendran J, *et al*. A metabolic remodeling in right ventricular hypertrophy is associated with decreased angiogenesis and a transition from a compensated to a decompensated state in pulmonary hypertension. *J Mol Med (Berl)* 2013;91:1315–1327.
15. Bogaard HJ, Natarajan R, Mizuno S, Abbate A, Chang PJ, Chau VQ, *et al*. Adrenergic receptor blockade reverses right heart remodeling and dysfunction in pulmonary hypertensive rats. *Am J Respir Crit Care Med* 2010;182:652–660.
16. Nadeau V, Potus F, Boucherat O, Paradis R, Tremblay E, Iglarz M, *et al*. Dual ET_A/ET_B blockade with macitentan improves both vascular remodeling and angiogenesis in pulmonary arterial hypertension. *Pulm Circ* 2018;8:2045893217741429.
17. Sun XQ, Zhang R, Zhang HD, Yuan P, Wang XJ, Zhao QH, *et al*. Reversal of right ventricular remodeling by dichloroacetate is related to inhibition of mitochondria-dependent apoptosis. *Hypertens Res* 2016;39:302–311.
18. Graham BB, Koyanagi D, Kandasamy B, Tuder RM. Right ventricle vasculature in human pulmonary hypertension assessed by stereology. *Am J Respir Crit Care Med* 2017;196:1075–1077.
19. Frump AL, Bonnet S, de Jesus Perez VA, Lahm T. Emerging role of angiogenesis in adaptive and maladaptive right ventricular remodeling in pulmonary hypertension. *Am J Physiol Lung Cell Mol Physiol* 2018;314:L443–L460.
20. Wei H, Bedja D, Koitabashi N, Xing D, Chen J, Fox-Talbot K, *et al*. Endothelial expression of hypoxia-inducible factor 1 protects the murine heart and aorta from pressure overload by suppression of TGF-β signaling. *Proc Natl Acad Sci USA* 2012;109:E841–E850.
21. Shiojima I, Sato K, Izumiya Y, Schiekofer S, Ito M, Liao R, *et al*. Disruption of coordinated cardiac hypertrophy and angiogenesis contributes to the transition to heart failure. *J Clin Invest* 2005;115: 2108–2118.
22. Eisele JC, Schaefer IM, Randel Nyengaard J, Post H, Liebetanz D, Brüel A, *et al*. Effect of voluntary exercise on number and volume of cardiomyocytes and their mitochondria in the mouse left ventricle. *Basic Res Cardiol* 2008;103:12–21.
23. Nemkov T, Hansen KC, D'Alessandro A. A three-minute method for high-throughput quantitative metabolomics and quantitative tracing experiments of central carbon and nitrogen pathways. *Rapid Commun Mass Spectrom* 2017;31:663–673.
24. Abe K, Toba M, Alzoubi A, Ito M, Fagan KA, Cool CD, *et al*. Formation of plexiform lesions in experimental severe pulmonary arterial hypertension. *Circulation* 2010;121:2747–2754.
25. Toba M, Alzoubi A, O'Neill KD, Gairhe S, Matsumoto Y, Oshima K, *et al*. Temporal hemodynamic and histological progression in Sugen5416/hypoxia/normoxia-exposed pulmonary arterial hypertensive rats. *Am J Physiol Heart Circ Physiol* 2014;306: H243–H250.
26. Howard CV, Reed MG. Unbiased stereology: three-dimensional measurement in microscopy. 2nd ed. Abingdon, UK: BIOS Scientific Publishers; 2005.
27. Piao L, Fang YH, Parikh K, Ryan JJ, Toth PT, Archer SL. Cardiac glutaminolysis: a maladaptive cancer metabolism pathway in the right ventricle in pulmonary hypertension. *J Mol Med (Berl)* 2013;91: 1185–1197.
28. Varghese AJ, Gulyas S, Mohindra JK. Hypoxia-dependent reduction of 1-(2-nitro-1-imidazolyl)-3-methoxy-2-propanol by Chinese hamster ovary cells and KHT tumor cells in vitro and in vivo. *Cancer Res* 1976; 36:3761–3765.
29. Graham BB, Chabon J, Gebreab L, Poole J, Debella E, Davis L, *et al*. Transforming growth factor-β signaling promotes pulmonary hypertension caused by *Schistosoma mansoni*. *Circulation* 2013; 128:1354–1364.
30. Kolb TM, Peabody J, Baddoura P, Fallica J, Mock JR, Singer BD, *et al*. Right ventricular angiogenesis is an early adaptive response to chronic hypoxia-induced pulmonary hypertension. *Microcirculation* 2015;22:724–736.
31. Graham BB, Chabon J, Kumar R, Kolosionek E, Gebreab L, Debella E, *et al*. Protective role of IL-6 in vascular remodeling in *Schistosoma* pulmonary hypertension. *Am J Respir Cell Mol Biol* 2013;49: 951–959.
32. Thomlinson RH, Gray LH. The histological structure of some human lung cancers and the possible implications for radiotherapy. *Br J Cancer* 1955;9:539–549.
33. Kane GC, Sachdev A, Villarraga HR, Ammash NM, Oh JK, McGoon MD, *et al*. Impact of age on pulmonary artery systolic pressures at rest and with exercise. *Echo Res Pract* 2016;3: 53–61.
34. Carmeliet P, Dor Y, Herbert JM, Fukumura D, Brusselmans K, Dewerchin M, *et al*. Role of HIF-1α in hypoxia-mediated apoptosis, cell proliferation and tumour angiogenesis. *Nature* 1998;394: 485–490.
35. De Bock K, Georgiadou M, Schoors S, Kuchnio A, Wong BW, Cantelmo AR, *et al*. Role of PFKFB3-driven glycolysis in vessel sprouting. *Cell* 2013;154:651–663.
36. Manavski Y, Lucas T, Glaser SF, Dorsheimer L, Günther S, Braun T, *et al*. Clonal expansion of endothelial cells contributes to ischemia-induced neovascularization. *Circ Res* 2018;122: 670–677.
37. Oikawa M, Kagaya Y, Otani H, Sakuma M, Demachi J, Suzuki J, *et al*. Increased [^{18}F]fluorodeoxyglucose accumulation in right ventricular free wall in patients with pulmonary hypertension and the effect of epoprostenol. *J Am Coll Cardiol* 2005;45: 1849–1855.
38. Lundgrin EL, Park MM, Sharp J, Tang WH, Thomas JD, Asosingh K, *et al*. Fasting 2-deoxy-2-[^{18}F]fluoro-D-glucose positron emission tomography to detect metabolic changes in pulmonary arterial hypertension hearts over 1 year. *Ann Am Thorac Soc* 2013;10: 1–9.
39. Ohira H, deKemp R, Pena E, Davies RA, Stewart DJ, Chandy G, *et al*. Shifts in myocardial fatty acid and glucose metabolism in pulmonary arterial hypertension: a potential mechanism for a maladaptive right ventricular response. *Eur Heart J Cardiovasc Imaging* 2016;17: 1424–1431.

40. Fang W, Zhao L, Xiong CM, Ni XH, He ZX, He JG, *et al*. Comparison of ^{18}F-FDG uptake by right ventricular myocardium in idiopathic pulmonary arterial hypertension and pulmonary arterial hypertension associated with congenital heart disease. *Pulm Circ* 2012;2:365–372.
41. Hemnes AR, Brittain EL, Trammell AW, Fessel JP, Austin ED, Penner N, *et al*. Evidence for right ventricular lipotoxicity in heritable pulmonary arterial hypertension. *Am J Respir Crit Care Med* 2014;189:325–334.
42. Talati MH, Brittain EL, Fessel JP, Penner N, Atkinson J, Funke M, *et al*. Mechanisms of lipid accumulation in the bone morphogenetic protein receptor type 2 mutant right ventricle. *Am J Respir Crit Care Med* 2016;194:719–728.
43. Legchenko E, Chouvarine P, Borchert P, Fernandez-Gonzalez A, Snay E, Meier M, *et al*. PPARγ agonist pioglitazone reverses pulmonary hypertension and prevents right heart failure via fatty acid oxidation. *Sci Transl Med* 2018;10:eaao0303.
44. Hsu S, Kokkonen-Simon KM, Kirk JA, Kolb TM, Damico RL, Mathai SC, *et al*. Right ventricular myofilament functional differences in humans with systemic sclerosis-associated versus idiopathic pulmonary arterial hypertension. *Circulation* 2018;137:2360–2370.
45. Katz WE, Gasior TA, Quinlan JJ, Lazar JM, Firestone L, Griffith BP, *et al*. Immediate effects of lung transplantation on right ventricular morphology and function in patients with variable degrees of pulmonary hypertension. *J Am Coll Cardiol* 1996;27:384–391.